minerals

MDPI

Article

Properties of Conglomerates from the Middle Ordovician Dongchong Formation and Its Response to the Yunan Orogeny in the Yunkai Area, South China

Zhihong Wang [1,2,*], Zhihong Li [2], Zhijun Niu [1,2], Chu'an Li [3], Hao Chen [4], Xiaoming Lin [5], Kun Hu [5] and Huazhou Yao [1,2]

[1] Hubei Key Laboratory of Paleontology and Geological Environment Evolution, Wuhan 430205, China
[2] Wuhan Center, China Geological Survey (Geosciences Innovation Center of Central South China), Wuhan 430205, China
[3] Guangdong Marine Geological Survey Institute, Guangzhou 510080, China
[4] Jiangxi Institute of Applied Science and Technology, Nanchang 330100, China
[5] Guangdong Geologic Survey Institute, Guangzhou 510080, China
* Correspondence: wzhihong@mail.cgs.gov.cn

Abstract: The strata in the Shita Mountain, Yunkai region, are predominantly composed of clastic rocks with intercalated limestones. However, the precise stratigraphic age remains uncertain due to the scarcity of fossils. Previously, conglomerate layers in this region were considered indicative of the Yunan Orogeny during the Cambrian–Ordovician transition. However, through the identification of 12 lithofacies types and 5 lithofacies combinations in the conglomerate layers of the Shita Mountain section, it has been confirmed that these layers represent a fan delta depositional environment characterized by debris flow, traction flow, torrent, and rock flow. Based on the presence of brachiopod fossils dating to the Early–Middle Ordovician, we propose a novel two-episode model for the Yunan Orogeny. The first episode corresponds to submarine fan deposition, while the second episode involves tectonic uplift and a short-term sedimentary hiatus. Further analysis of the detrital zircon provenance reveals a strong affinity among the Yunkai area, India, Antarctica, the Lhasa, the Himalayas, Southern Qiangtang, and Western Australia during the Early–Middle Ordovician transition under the Gondwana assemblage background.

Keywords: Yunan orogeny; Yunkai area; Ordovician; South China; conglomerates; detrital zircons

check for updates

Citation: Wang, Z.; Li, Z.; Niu, Z.; Li, C.; Chen, H.; Lin, X.; Hu, K.; Yao, H. Properties of Conglomerates from the Middle Ordovician Dongchong Formation and Its Response to the Yunan Orogeny in the Yunkai Area, South China. *Minerals* **2023**, *13*, 998. https://doi.org/10.3390/min13080998

Academic Editors: Giovanni Martinelli and Nigel J. Cook

Received: 7 June 2023
Revised: 11 July 2023
Accepted: 26 July 2023
Published: 28 July 2023

Copyright: © 2023 by the authors. Licensee MDPI, Basel, Switzerland. This article is an open access article distributed under the terms and conditions of the Creative Commons Attribution (CC BY) license (https://creativecommons.org/licenses/by/4.0/).

1. Introduction

The South China Block (SCB) consists of the Yangtze and Cathaysia Blocks (Figure 1A), which amalgamated along the Jiangnan Orogen during the Neoproterozoic period [1–4]. In recent years, numerous studies on litho-geochemistry and detrital zircon provenance have provided compelling evidence for the connectivity or adjacency of the Yangtze, Cathaysia, and Gondwana blocks during the late Neoproterozoic to early Paleozoic periods [1,5–11]

The Ordovician period played a significant role in the early Paleozoic Orogeny in South China, as it witnessed notable variations in sedimentary formations and paleontological fauna [12]. Mo [13] suggested that there was a parallel unconformity between the Lower Ordovician Suoweiling Group and the Cambrian Bacun Group, which represented the first episode of the early Paleozoic orogeny and was named the Yunan Orogeny. Since then, the Yunan Orogeny has been widely quoted and elaborated [9,11,14–16]. The derivation of detritus suggests that South China was located at the nexus between India, Antarctica, and Australia, along the northern margin of East Gondwana during the Cambrian–Ordovician transition [9,10]. The orogeny during the Cambrian–Ordovician transition, which is widely distributed along the northern margin of Gondwana, may represent the Kuunga collision belt between the Australian and Indian–East Antarctic plates for the consolidation of Gondwana. The collision zone runs northward from Prydz Bay of Antarctica to the northeastern

margin of the Himalayas and the western margin of Australia and extends to the southern margin of South China. In addition, the Yunan Orogeny may be a specific manifestation of this great orogenic event in South China [9].

The Yunan–Deqing in the Yunkai area, after which the Yunan Orogeny was named, represents a key locality for studying the evolution of early Paleozoic orogeny in South China (Figure 1B). Despite extensive discussions on the geological record and manifestation characteristics of the Yunan Orogeny, there has been ongoing controversy due to poor outcrop exposures and stratigraphic dating constraints. In our recent years of investigation in the region, we discovered previously unknown fossil preservation sites, which have provided us with a different understanding of the stratigraphic age. Additionally, we observed conglomerate layers near the fossil-bearing horizons. These findings have led us to reevaluate the geological evolutionary history of this area and have offered new insights into the processes of the Yunan Orogeny. The aim of this study is to investigate the conglomerate layers in the Yunan region and propose novel perspectives on the Yunan Orogeny and its implications from a stratigraphic and sedimentological standpoint.

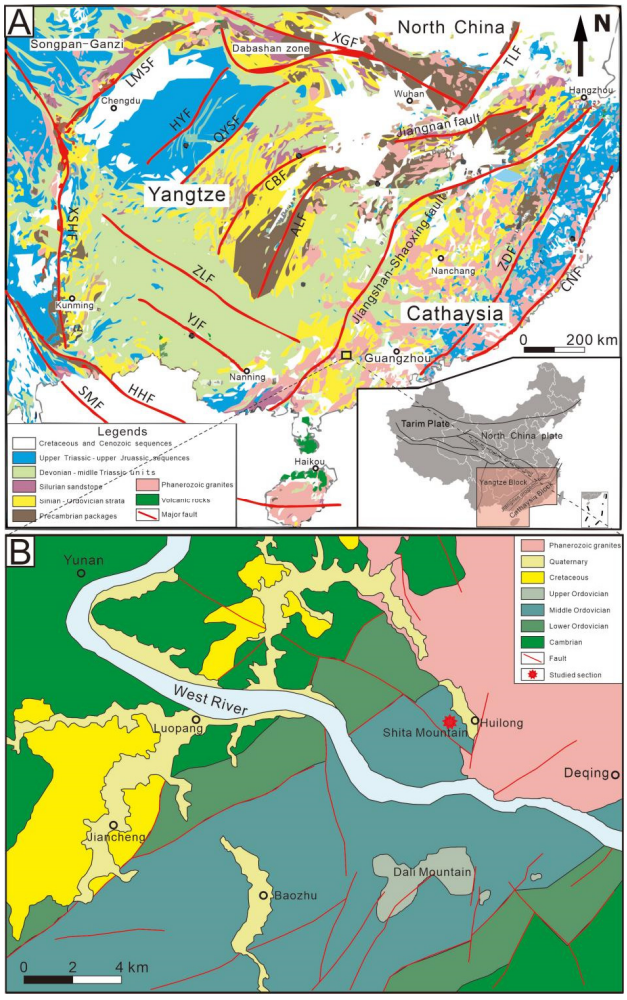


Figure 1. (**A**) Simplified geological map of South China Block (modified from [4]) and (**B**) simplified geological map of Yunan–Deqing area showing the location of the section presented in Figure 2. (SMF: Song-Ma Fault, HHF: Honghe Fault, XSHF: Xianshuihe Fault, LMSF: Longmenshan Fault, HYSF: Huayingshan Fault, QYSF: Qiyueshan Fault, CBF: Cili–Baojing Fault; ALF: Anhua–Luocheng Fault; ZLF: Ziyun–Luodian Fault; YJF: Youjiang Fault; XGF: Xiangfan–Fuangxi Fault; TLF: Tan–Lu Fault; ZDF: Zhenghe–Dapu Fault; CNF: Changle–Nanao Fault).

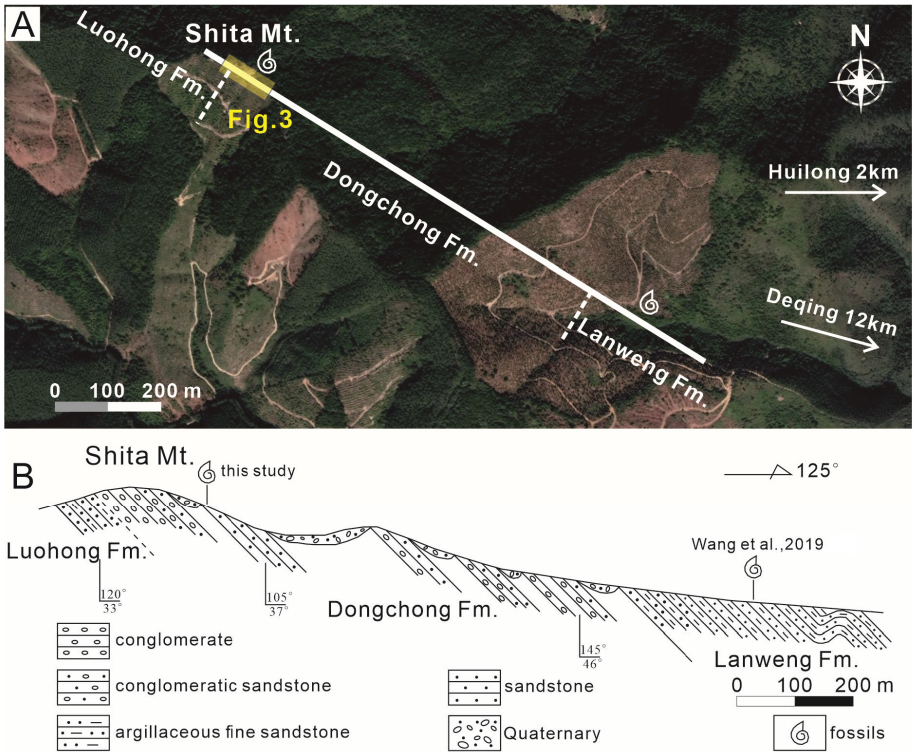


Figure 2. (**A**) Image from Google Earth showing the measured section's location at Shita Mountain and (**B**) the geological cross-section of the Ordovician strata (the two fossil localities are respectively referred to this study and Wang et al. 2019 [17]).

2. Geological Background

The SCB, an important continental plate in eastern Asia, underwent extensive tectono-magmatic activities during the early Paleozoic Wuyi–Yunkai orogeny. This orogeny is named after the Wuyi and Yunkai areas in South China, which exhibit a high concentration of early Paleozoic magmatic rocks. The Yunkai area in the early Paleozoic period exhibited a relatively complete exposure of sedimentary formations, which were predominantly composed of clastic rocks interbedded with minor amounts of carbonate rocks. However, due to subsequent strong tectonic-magmatic activities and complex metamorphic deformation, particularly with limited research on biota, the lack of a high-precision chronostratigraphic framework, and unclear correlation markers in clastic rock assemblages, a profound understanding of this area has been impeded.

A sequence of early to mid-Neoproterozoic accretionary arc complexes helped to construct and accrete the Archean and Paleoproterozoic basement units that make up the Cathaysia Block at the northern edge of Gondwana [18,19]. The Neoproterozoic succession is overlain by lower Paleozoic strata, displaying significant facies variations across the Cathaysia Block. The Cambrian and Ordovician strata are predominantly composed of siliciclastic sediments with minor interbedded carbonate deposits [20]. These strata exhibit a variety of sedimentary structures, including rhythmic bedding, cross-bedding, and wavy scour marks, suggesting deposition in a littoral-neritic environment [21]. In general, Silurian sequences are not widely preserved within the Cathaysia Block, except for the Qinzhou–Fangchenggang area in the south. Within the Yunkai area of the Cathaysia Block, there is a limited occurrence of unconformity surfaces within the early Paleozoic succession, notably including the presence of a disconformity between the Cambrian and Ordovician strata [11]. Within these sedimentary records, remarkably well-preserved sedimentary features are retained, enabling geologists to reconstruct paleocurrent directions during that period. Paleocurrent analysis, which is closely associated with provenance, plays a pivotal role in deciphering the orientation of the current system responsible for the

dispersion and deposition of sedimentary rock units. This analysis can be conducted by examining scalar properties of the sediment or by evaluating vectoral directional elements within it. The predominant paleocurrent orientations inferred from the early Paleozoic successions in the western Cathaysia region indicate a northwestern direction [21,22]. Consequently, it can be deduced that the prevailing paleocurrent direction in most regions of the Cathaysia Block was predominantly northwestward.Systematic research on the Ordovician in the Yunkai area commenced in 1962 with the publication of the Geological Map of the Luoding Region (1:200,000). This initial mapping effort classified the Ordovician strata into the Huilong Group, Suoweiling Group, and Sanjian Group. Subsequently, in 1977, during the compilation of the 1:500,000 Geological Map of Guangdong Province, new fossil evidence led to the revision of the Huilong Group's age as Late Cambrian. As a result, the Ordovician strata were reclassified into the Early Ordovician Shuweiling Group and the Middle–Late Ordovician Sanjian Group. Further advancements came from the Deqing–Yuecheng geological survey (1:50,000) conducted in 1992 by the Guangdong Regional Geological Survey Team. They proposed a revised classification for the Ordovician strata, including the Luohong, Luodong, Dongchong, and Lanweng Formations, which are still used today. The Luodong Formation represents a partially exposed limestone unit within the region.

Recent fossil collections have significantly enhanced the understanding of the lithostratigraphic and biostratigraphic sequences of the Ordovician period in the studied area [12,17,23,24]. The Ordovician in the Deqing area is mainly composed of flyschoidal clastics with locally intercalated limestone, multi-layered conglomerate, gravel-bearing sandstone, and medium-fine-grained quartz sandstone interposed between medium-thin layers of silt. Several layers of conglomerate rock have been observed in the basal part of the Ordovician units [23]. In this study, the Ordovician strata section was measured near Huilong town, Deqing County (Figure 2A). The discovery of several Middle Ordovician brachiopod fossils within the strata of the Dongchong Formation has provided valuable insights into the dynamics of the Yunan Orogeny in South China, particularly in the Cathaysia.

3. Materials and Methods

A total of 12 outcrops were observed and one section was logged using sedimentary facies analysis. As a result, a novel lithostratigraphic framework for the Ordovician section was established, as depicted in Figure 2B.

This study specifically investigates the lower part of the Dongchong Formation. Through a comprehensive analysis of lithological variations, a total of 12 distinct lithofacies and 5 lithofacies associations were identified. The fieldwork encompassed meticulous mapping of the section, enabling the establishment of a detailed lithological log that summarizes the characteristics observed within the studied area (Figure 3). The identification of the sedimentary lithofacies was performed as described by Miall [25,26]. Facies identifications and interpretations were based on a detailed examination of color, texture, composition, sedimentary structures, and bedding characteristics.

In the process of fossil excavation, two fossil sites were found. One was at the lower part of the Dongchong Formation (Figure 2B, this study) and the other was at the upper Ordovician of the Lanweng Formation (reported by [17]). Three brachiopod fossils from the Dongchong Formation were identified. All figured specimens are kept in the Wuhan Center, China Geological Survey.

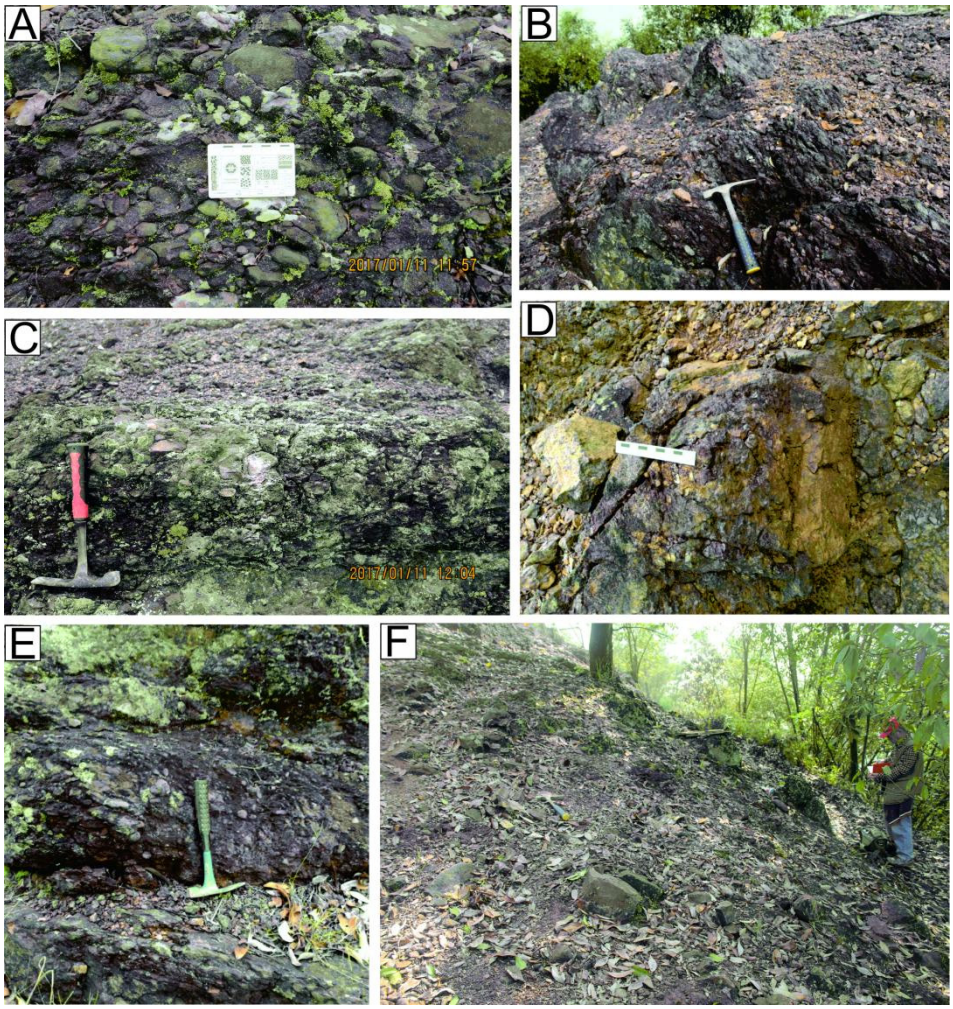


Figure 3. Outcrops of basal part of the Dongchong Formation at Shita Mountain, Deqing, western Guangdong: (**A**) conglomerates in lower part of Bed 8; (**B**) conglomerates in upper part of Bed 8; (**C**,**D**) conglomerates interbedded with sandstones in Bed 9; (**E**) conglomerates in lower part of Bed 10; (**F**) coarse sandstone in upper part of Bed 10 (geological hammer = ca., 30 cm).

One surrounding sandstone rock sample of the conglomerate analyzed in this study was collected from the basal Dongchong Formation for U–Pb dating of detrital zircons. A total of 80 analyses were made on 80 individual zircon grains yielding 79 concordant ages. Zircons were separated by conventional heavy liquid and magnetic techniques. A random selection of grains was mounted in epoxy resin, sectioned approximately in half, and polished. Zircon U–Pb dating was conducted using LA-ICPMS in Nanjing Hongchuang Exploration Technology Service Co., Ltd. The Resolution SE model laser ablation system (Applied Spectra, Carlsbad, CA, USA) was equipped with an ATL (ATLEX 300) excimer laser and a Two Volume S155 ablation cell. The laser ablation system was coupled to an Agilent 7900 ICPMS (Agilent, Santa Clara, CA, USA). Detailed tuning parameters can be seen in Thompson et al. [27]. LA-ICPMS tuning was performed using a 50-micron-diameter line scan at 3 µm/s on an NIST 612 at ~3.5 J/cm^2 with a repetition rate of 10 Hz. The gas flow was adjusted to obtain the highest sensitivity (^{238}U~6 × 10^5 cps) and the lowest oxide ratio (ThO/Th < 0.2%). P/A calibration was conducted on the NIST 610 using a 100-micron-diameter line scan. Other laser parameters were the same as that of tuning. Pre-ablation was conducted for each spot analysis using 5 laser shots (~0.3 µm in depth) to remove potential surface contamination. The analysis was performed using a 30 µm diameter spot at 5 Hz with a fluence of 2.5 J/cm^2. The Iolite software package was used for data reduction [28]. The Zircon 91500 and GJ-1 were used as primary and

secondary reference materials, respectively. Triplets of 91500 and GJ-1 were bracketed between multiple groups of 10 to 12 sample unknowns. Typically, 35–40 s of the sample signals was acquired after 20 s gas background measurement. The exponential function was used to calibrate the downhole fractionation [28]. NIST 610 and ^{91}Zr were used to calibrate the trace element concentrations as the external reference material and internal standard element, respectively. Measured ages of 91500 (1061.5 ± 3.2 Ma, 2σ) and GJ-1 (604 ± 6 Ma, 2σ) were well within 1% of the accepted age.

4. Result

The measured section (GPS:23°11′34″ N, 111°40′09″ E) is located on Shita Mountain about 12 km northwest of Deqing County. The sedimentary characteristics of the section are shown in Figure 3, and Beds 8–10 are the key horizons in this study.

4.1. Characteristics of Conglomerates in the Lower Part of Dongchong Formation

The lithology of the Dongchong Formation primarily consists of yellow-brown to brownish-yellow medium-bedded (locally thick-bedded) quartz sandstone, feldspar quartz sandstones, and quartzose sandstones interbedded with gray-green, brownish-yellow, and purple-red thin- to medium-bedded silty sandstones, siltstones, and mudstones. In general, the Dongchong Formation is characterized by the development of cyclic sequences composed of quartz sandstones, siltstones, and mudstones. The lower part of the coarse clastic rocks exhibits distinct normal grading, while upward, rhythmic bedding, ripple bedding, and parallel bedding sedimentary structures are observed. Overall, there is a fining of grain size and an increase in the proportion of muddy components from the bottom to the top.

The basal part is typically marked by the occurrence of limestone lenses or thick-bedded conglomerates and sandstones, and it is in unconformable contact with the underlying strata. A well-defined, normal-graded bedding is commonly developed in the coarse clastic rocks at the base. From the bottom to the top, there is a general fining upward trend with an increase in mud content, exhibiting distinct characteristics of a retrograding sequence. The sedimentary succession of the studied conglomerate layer is 27 m thick and is well exposed along the mountain ridge. Below are the detailed descriptions.

Bed 8, with a thickness of 6 m, comprises reddish-purple medium-layered cobbles, interspersed with a bedding of pebbles in the middle. The cobbles exhibit particle size ranging from approximately 4~8 cm, while the pebbles have an average particle size of 2~3 cm. The predominantly grain-supported conglomerate exhibits a relatively simple composition, consisting of rounded to subrounded gravels with moderate sorting. The reddish-purple argillaceous siltstones play a significant role as cementing agents. A distinct erosional surface is evident at the base of this layer, indicating a sedimentary hiatus and separating it from the underlying Luohong Formation.

The thickness of Bed 9 is 12 m. The lower part of this layer is composed of reddish pebbles, displaying particle sizes ranging from 2.5~5 cm and exhibiting a graded bedding. It comprises gravels from the underlying Luohong Formation that are subrounded to rounded, have a matrix-supported structure, and contain sand and muddy sediments between them. The upper part of Bed 9 comprises purplish-red massive mixed cobbles, featuring larger particle size of up to 25 cm, which are commonly around 12~15 cm. The middle part of this layer exhibits coarse-tailed graded bedding, while its bottom is characterized by erosion structures.

A layer nine-meters-thick covers Bed 10, which is mostly composed of reddish medium-bedded granules and gravel-bearing sandstones with few intercalated, thin-bedded gravelly sandstones. The particle size of moderately sorted gravels is mainly around 3~4 mm. These gravels in general exhibit a subrounded shape, although a few of them are subangular. The composition of the gravels primarily consists of argillaceous siltstones and sandstones, with a small amount of quartz gravels. Erosion-related structures

are at the bottom of this layer. Compared to Beds 8 and 9, the gravels of Bed 10 are not only small in volume but also dominated by single-component gravels.

4.2. Lithofacies Types and Facies Associations

Based on our investigations, in the conglomerate layer of Beds 8–10 at the top of Shita Mountain, 12 types of lithofacies could be identified (Table 1), which could be classified into 5 types of lithofacies associations (Figure 4), as described in detail below.

Table 1. Description and interpretation of the lithofacies of Beds 8–10 for the studied section.

Facies Code *	Lithofacies	Sedimentary Structures	Interpretation
Gc	both well- and poorly sorted grains	massive or horizontal stratification	longitudinal bars in the braided river channel
Gms	Matrix-supported gravel	none	debris flow deposits
Gcm	clast-supported massive gravel	cross-stratified, matrix-supported conglomerate	traction by a unidirectional current
Gm	massive or crudely bedded gravel, clast-supported gravel	horizontal bedding, imbrication	sieve deposits, channel-lag deposits
Gmg	Matrix-supported gravel	inverse to normal grading	pseudoplastic debris flow (low strength, viscous)
Gi	conglomerate with well-sorted and rounded clasts.	imbrication	longitudinal bars
Sh	parallel layered sandstones	horizontal or flat bedding	lower flow regime plane bed
Gg	granule to massive gravel	chaotic deposits, poorly sorted.	longitudinal bedforms
Gt	gravel, stratified	trough cross-bed imbrication	minor channel fills
Gp	gravel, stratified	planar cross-beds	linguoid bars or deltaic growths from older bar remnants
Fl	sand, silt, mud, interbedded	Ripple-laminated or undulatory bedding	waning flow
Fm	clay, silt	massive	drape deposits

* Lithofacies codes of Miall [25,26].

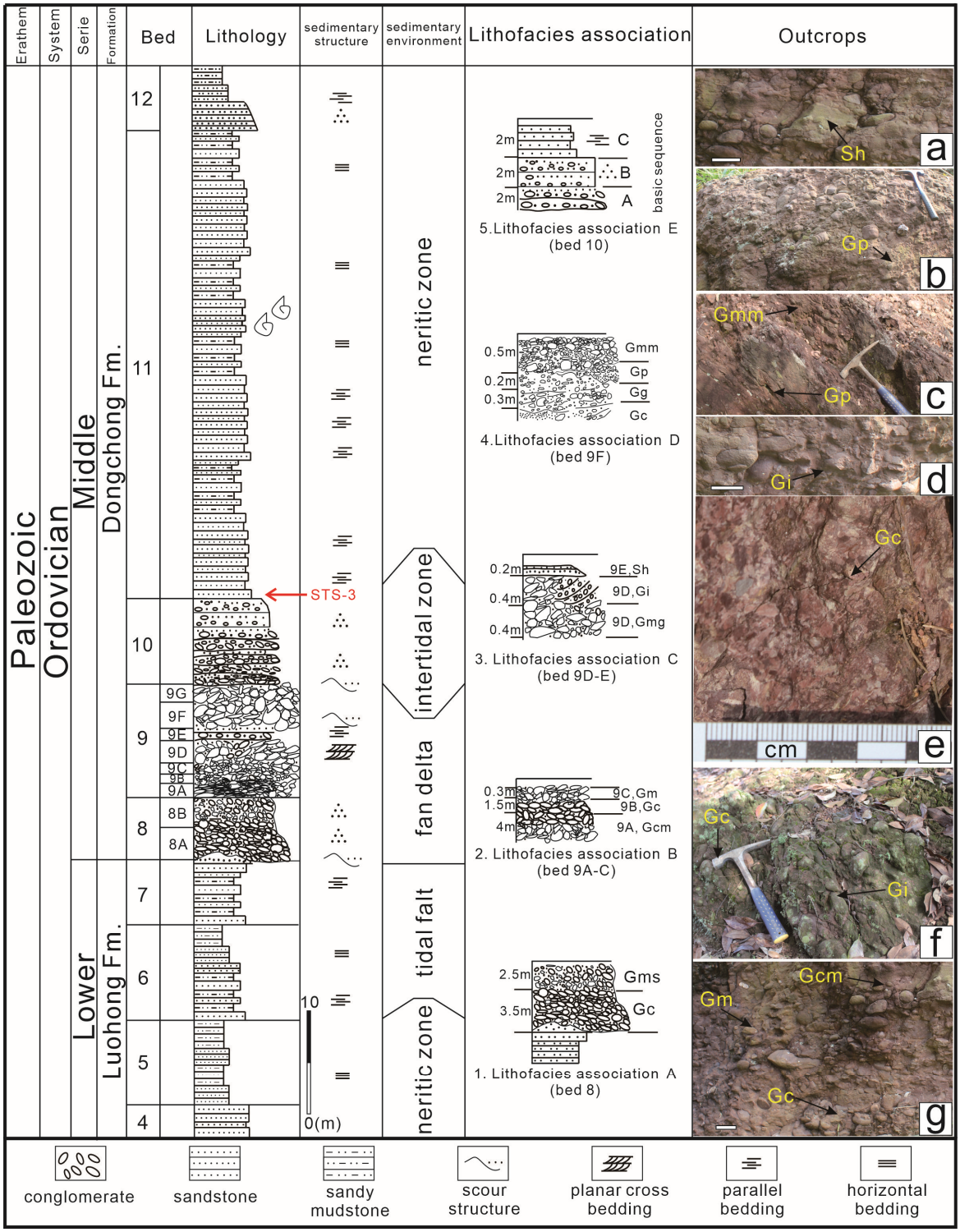


Figure 4. The lithology and lithofacies association of the Ordovician upper Luohong Formation and lower Dongchong Formation in Shita Maintain, Deqing, Guangdong. The length of the white bar is 10 cm, and the hammer is 30 cm. The photos (**a**–**g**) showcase characteristic lithofacies features observed in various field outcrops.

4.2.1. Lithofacies Association A

This lithofacies association is recognized in Bed 8 with a thickness of 6 m. The lower 8A layer is composed of grain-supported conglomerate facies (Gc) and the upper 8B layer is composed of sandy-matrix-supported conglomerate facies (Gms) to form complete channel

deposits. These channel deposits exhibit lenticular bodies or thick tabular sheets with intricate bedding geometries and erosive bases.

4.2.2. Lithofacies Association B

Within association B, three lithofacies types are distinguished: (1) massive, clast-supported gravel facies (Gcm); (2) grain-supported conglomerate facies (Gc); and (3) massive-bedded clast-supported gravel facies (Gm). This lithofacies association is 5.8 thick, is seen in Bed 9 (A–C), and represents debris-flow and flood-flow deposits in an alluvial fan. The sedimentary structure observed corresponds to a poorly stratified clast-supported conglomerate. It consists of alternating centimeter-thick horizons characterized by pebbles to small clast-supported cobbles, as well as gravely to pebbly sandy layers. These units exhibit a lateral extent and can be observed with either horizontal bedding or large-scale slightly dipping sigmoidal foresets.

4.2.3. Lithofacies Association C

Lithofacies association C occurs in Bed 9 (D–E) of the studied section and includes (1) gravel-supported float conglomerate facies (Gmg), (2) imbricated conglomerate facies (Gi), and (3) parallel sandstone-bedding facies.

The lower part of Bed 9D belongs to Gmg facies, which is composed of purplish-red massive cobble/pebble stones and gravel-bearing sandstones. The conglomerate within the pebbly sandstones is clast-supported and exhibits subangular to subrounded shapes with moderate sorting, with gravels ranging in particle size from 2~6 cm (median of 4 cm). In terms of matrix content, it is about 20~25%, while the gravel content is about 75~80% with a thickness of 0.4 m.

The upper part of Bed 9D belongs to well-sorted pebbles, moderately sorted gravel (Gi) facies, and flat-shaped gravels, particle size ranging from 4~6 cm and dipping north-eastward at 28~30°. Either matrix-supported or grain-supported structures are visible. Purple-reddish sandstones constitute the gravel composition. It makes up about 15~20% of the matrix content, while the gravel content is about 80~85% with a thickness of 0.4 m.

Bed 9E, which is 0.2 m thick, shows horizontally bedded, medium-to-coarse sandstone (Sh) facies and is composed of yellow-green, medium-fine grained sandstones to fine sandstones with lens-like distributions and parallel bedding. Fine gravels can be found at the bottom of this layer. Sandstones and siltstones are the main components of the gravels, which show an oval or round shape and are moderately sorted.

Association C represents a well-defined sedimentary sequence exhibiting a clear transition from debris-flow deposits to braided-river facies, culminating in the formation of a central bar. The depositional environments within association C are arranged in a distinct bottom-to-top sequence, indicating a progressive shift in sedimentary processes and hydrodynamic conditions over time.

4.2.4. Lithofacies Association D

Lithofacies association D is recognized in Bed 9 (F–G) and is made up of thin pebble layers (Gc), granule-to-massive gravels (Gg), and medium-to-large-scale trough cross-bedded gravel (Gt) facies. Bed 9F is about 1 m thick and is composed of purple-red massive coarse and medium-grained conglomerate. It is well observed that the gravel particle size is uneven, whose cloud varies from 8 cm to as large as 22 cm. A positive sequence is noted in the gravels, accompanied by abundant sandstones and few quartz gravels, and there is a scour structure at the bottom. The sedimentary characteristics indicate the presence of debris flow during the flood stage.

4.2.5. Lithofacies Association E

This lithofacies association is distributed in Bed 10 with a graded conglomerate (Gg), planar cross-bedding conglomerate (Gp), parallel layered sandstones (Sh), and fine-laminated siltstone (Fl) facies. The sedimentary structures include positive-grained pro-

gressive bedding and erosion surfaces. The lower part of the sedimentary succession is dominated by gravels, which are subrounded and well sorted. The sequences show thinning and fining trends vertically upward on an outcrop scale. These sediments are characterized by the presence of small-scale ripple marks with low relief, which are formed by the action of tidal currents or waves.

4.3. Detrital Zircon U-Pb Ages of Dongchong Formation

Detrital zircon U-Pb ages were determined using 80 grains from the sandstone sample STS-3 (show in Figure 4) of Dongchong Formation, of which 79 detrital zircons display a 90% or greater concordance and range in ages from 2433 Ma to 521 Ma. Two major age groups are recognized at 1.2 to 0.9 Ga and 0.6 to 0.5 Ga, with distinct age peaks at 992 ± 8 Ma (MSWD = 5.2) and 526 ± 2 Ma (MSWD = 1.8) (Figure 5).

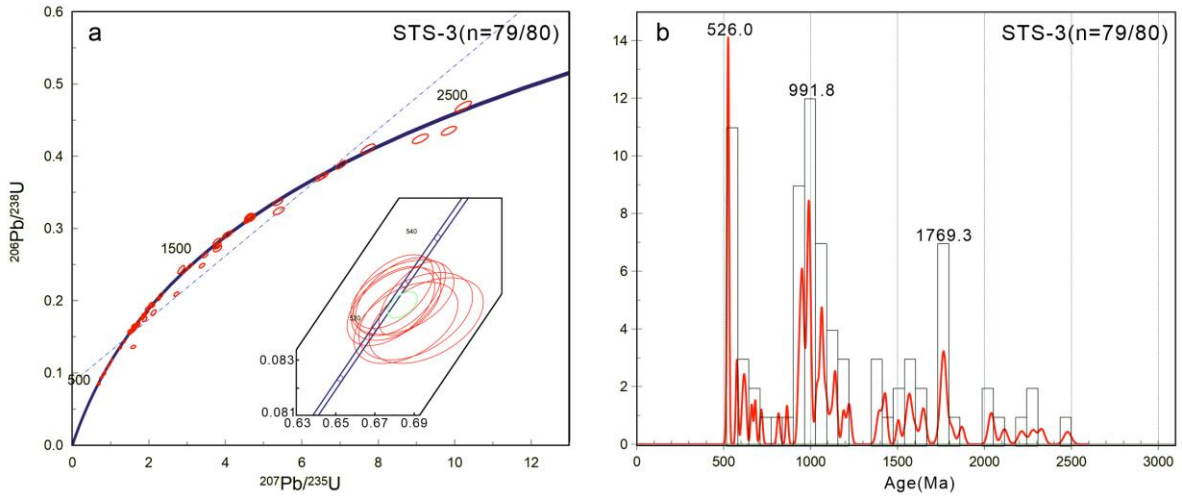


Figure 5. LA-ICP-MS zircon U-Pb concordia age plots and age histograms of zircons of STS-3 from the basal Dongchong Formation.

The LA-ICP-MS U-Pb data of the analyzed sample of this study are reported in Table 2. The interpreted ages are based on $^{206}Pb/^{238}U$ ages for <1000 Ma grains and $^{206}Pb/^{207}Pb$ ages for >1000 Ma grains [29].

Table 2. U-Pb data for detrital zircons from the Early–Middle Ordovician transition in the Shita Mountain, Western Guangdong.

Analysis	$^{207}Pb/^{206}Pb$		$^{207}Pb/^{235}U$		$^{207}Pb/^{238}U$		$^{207}Pb/^{206}Pb$		$^{207}Pb/^{235}U$		$^{206}Pb/^{238}U$		Th	U	Th/U	Concordance
	Ratio	1σ	Ratio	1σ	Ratio	1σ	Age	1σ	Age	1σ	Age	1σ	ppm	ppm		
SRM 610	0.92571	0.02747	28.30205	0.85328	0.22076	0.00366	/	/	3430	30	1286	19	548	542	1.01	9%
91500std	0.07564	0.00172	1.87626	0.04606	0.17900	0.00213	1087	46	1073	16	1062	12	32	85	0.37	98%
91500std	0.07412	0.00168	1.82414	0.03886	0.17934	0.00217	1056	51	1054	14	1063	12	32	85	0.37	99%
GJ-600	0.06075	0.00136	0.81456	0.01838	0.09723	0.00111	632	48	605	10	598	7	16	193	0.08	98%
GJ-600	0.06054	0.00125	0.81270	0.01696	0.09727	0.00100	633	72	604	10	598	6	16	190	0.08	99%
Ple-337	0.06687	0.00224	0.49985	0.01991	0.05302	0.00058	835	70	412	14	333	4	77	707	0.11	78%
STS-3–01	0.09384	0.00129	2.71752	0.04223	0.20910	0.00202	1506	26	1333	12	1224	11	80	214	0.37	91%
STS-3-02	0.06030	0.00174	0.69626	0.01925	0.08441	0.00101	613	63	537	12	522	6	216	113	1.92	97%
STS-3-03	0.05882	0.00210	0.68587	0.01752	0.08433	0.00096	561	78	530	11	522	6	306	172	1.78	98%
STS-3-04	0.12705	0.00140	6.56211	0.08561	0.37306	0.00338	2058	19	2054	12	2044	16	101	213	0.47	99%
STS-3-05	0.07804	0.00095	1.89155	0.03666	0.17418	0.00222	1148	24	1078	13	1035	12	51	792	0.06	95%
STS-3-06	0.12032	0.00192	5.39622	0.09371	0.32418	0.00337	1961	29	1884	15	1810	16	80	120	0.66	95%
STS-3-07	0.07328	0.00130	1.66175	0.03245	0.16390	0.00171	1022	35	994	12	978	10	100	148	0.67	98%
STS-3-08	0.08068	0.00126	2.30906	0.04384	0.20716	0.00273	1214	30	1215	14	1214	15	76	169	0.45	99%
Ple-337	0.05379	0.00104	0.40473	0.00884	0.05442	0.00066	361	44.4	345	6	342	4	43	500	0.09	98%
91500std	0.07302	0.00166	1.79953	0.04194	0.17893	0.00210	1015	46	1045	15	1061	12	31	85	0.37	98%
91500std	0.07674	0.00168	1.90087	0.04327	0.17941	0.00196	1115	48	1081	15	1064	11	31	83	0.37	98%

Table 2. *Cont.*

Analysis	$^{207}Pb/^{206}Pb$		$^{207}Pb/^{235}U$		$^{207}Pb/^{238}U$		$^{207}Pb/^{206}Pb$		$^{207}Pb/^{235}U$		$^{206}Pb/^{238}U$		Th	U	Th/U	Concordance
	Ratio	1σ	Ratio	1σ	Ratio	1σ	Age	1σ	Age	1σ	Age	1σ	ppm	ppm		
GJ-600	0.05988	0.00126	0.81340	0.01839	0.09829	0.00111	598	44	604	10	604	7	16	190	0.08	99%
STS-3-09	0.08485	0.00209	1.59216	0.04109	0.13582	0.00149	1322	47	967	16	821	8	140	100	1.40	83%
STS-3-10	0.06258	0.00080	0.93272	0.01367	0.10800	0.00117	695	27	669	7	661	7	344	884	0.39	98%
STS-3-11	0.10653	0.00134	4.61784	0.08385	0.31346	0.00444	1743	24	1753	15	1758	22	103	177	0.58	99%
STS-3-12	0.07036	0.00100	1.53051	0.02371	0.15741	0.00139	939	30	943	10	942	8	126	232	0.54	99%
STS-3-13	0.06057	0.00080	0.85680	0.01417	0.10229	0.00115	633	30	628	8	628	7	46	561	0.08	99%
STS-3-14	0.05908	0.00151	0.69088	0.01917	0.08456	0.00103	569	56	533	12	523	6	130	118	1.10	98%
STS-3-15	0.07462	0.00129	1.71112	0.03447	0.16576	0.00179	1057	30	1013	13	989	10	146	165	0.88	97%
STS-3-16	0.07424	0.00097	1.71385	0.02980	0.16695	0.00213	1048	26	1014	11	995	12	11	608	0.02	98%
SRM 610	0.91932	0.01130	28.37179	0.39321	0.22322	0.00195	/	/	3432	14	1299	10	548	542	1.01	9%
91500std	0.07388	0.00162	1.83199	0.04384	0.17962	0.00215	1039	44	1057	16	1065	12	31	84	0.37	99%
91500std	0.07588	0.00167	1.86841	0.04334	0.17872	0.00212	1092	49	1070	15	1060	12	32	85	0.37	99%
GJ-600	0.06123	0.00126	0.82277	0.01708	0.09763	0.00102	656	44	610	10	600	6	16	191	0.08	98%
STS-3-17	0.10100	0.00164	3.79664	0.07099	0.27203	0.00286	1643	30	1592	15	1551	15	44	101	0.44	97%
STS-3-18	0.07151	0.00157	1.57421	0.03565	0.16008	0.00174	972	44	960	14	957	10	57	119	0.48	99%
STS-3-19	0.13115	0.00134	7.03470	0.09457	0.38821	0.00386	2113	18	2116	12	2115	18	183	452	0.40	99%
STS-3-20	0.07424	0.00130	1.71619	0.03268	0.16759	0.00165	1048	35	1015	12	999	9	49	122	0.40	98%
STS-3-21	0.15787	0.00153	10.22251	0.14048	0.46871	0.00493	2433	16	2455	13	2478	22	402	300	1.34	99%
STS-3-22	0.10121	0.00132	4.07940	0.06205	0.29214	0.00284	1647	24	1650	13	1652	14	135	155	0.87	99%
STS-3-23	0.07177	0.00101	1.64309	0.02607	0.16591	0.00146	989	30	987	10	990	8	51	274	0.19	99%
STS-3-24	0.06918	0.00144	1.49848	0.03288	0.15750	0.00176	906	43	930	13	943	10	58	90	0.64	98%
Ple-337	0.05247	0.00092	0.39411	0.00780	0.05446	0.00059	306	41	337	6	342	4	70	706	0.10	98%
91500std	0.07618	0.00159	1.88543	0.04583	0.17940	0.00222	1100	43	1076	16	1064	12	32	87	0.37	98%
91500std	0.07358	0.00152	1.81497	0.04126	0.17894	0.00186	1031	43	1051	15	1061	10	32	85	0.37	99%
GJ-600	0.05837	0.00121	0.78541	0.01737	0.09780	0.00111	543	44	589	10	602	7	16	191	0.08	97%
STS-3-25	0.07048	0.00129	1.59739	0.03078	0.16479	0.00168	943	42	969	12	983	9	210	184	1.14	98%
STS-3-26	0.08799	0.00119	2.92341	0.04616	0.24115	0.00258	1383	21	1388	12	1393	13	215	199	1.08	99%
STS-3-27	0.07490	0.00101	1.95565	0.03236	0.18895	0.00195	1066	28	1100	11	1116	11	207	280	0.74	98%
STS-3-28	0.15537	0.00195	9.09972	0.13621	0.42411	0.00427	2406	21	2348	14	2279	19	59	64	0.93	97%
STS-3-29	0.09859	0.00124	3.75855	0.05404	0.27582	0.00249	1598	22	1584	12	1570	13	60	131	0.45	99%
STS-3-30	0.07520	0.00088	1.86156	0.02606	0.17907	0.00182	1074	24	1068	9	1062	10	207	472	0.44	99%
STS-3-31	0.10627	0.00143	4.60994	0.07645	0.31349	0.00355	1736	19	1751	14	1758	17	139	235	0.59	99%
STS-3-32	0.07831	0.00128	2.09801	0.03822	0.19344	0.00190	1155	33	1148	13	1140	10	149	189	0.79	99%
SRM 610	0.91517	0.01149	28.60076	0.36546	0.22599	0.00204	/	/	3440	13	1313	11	548	542	1.01	10%
91500std	0.07411	0.00169	1.82053	0.04195	0.17813	0.00197	1056	51	1053	15	1057	11	31	83	0.37	99%
91500std	0.07565	0.00157	1.87987	0.03870	0.18021	0.00208	1087	42	1074	14	1068	11	30	81	0.37	99%
GJ-600	0.06227	0.00124	0.83730	0.01710	0.09740	0.00106	683	43	618	9	599	6	16	192	0.08	96%
STS-3-33	0.07478	0.00131	1.86179	0.03546	0.18003	0.00196	1063	35	1068	13	1067	11	188	164	1.15	99%
STS-3-34	0.05745	0.00104	0.67946	0.01349	0.08544	0.00087	509	36	526	8	529	5	81	247	0.33	99%
STS-3-35	0.07629	0.00092	1.89719	0.02492	0.17967	0.00136	1103	24	1080	9	1065	8	99	391	0.25	98%
STS-3-36	0.07248	0.00104	1.59182	0.02387	0.15893	0.00137	1000	29	967	9	951	8	130	492	0.26	98%
STS-3-37	0.07073	0.00091	1.61987	0.02387	0.16574	0.00159	950	26	978	9	989	9	303	404	0.75	98%
STS-3-38	0.09543	0.00131	3.46423	0.05106	0.26287	0.00219	1537	26	1519	12	1505	11	87	135	0.64	99%
STS-3-39	0.10706	0.00142	4.64561	0.07386	0.31435	0.00350	1750	25	1758	13	1762	17	110	302	0.36	99%
STS-3-40	0.10696	0.00146	4.66704	0.06959	0.31622	0.00284	1750	25	1761	13	1771	14	104	188	0.56	99%
Ple-337	0.05273	0.00113	0.39126	0.00887	0.05380	0.00054	317	16	335	6	338	3	45	520	0.09	99%
91500std	0.07609	0.00176	1.88790	0.04659	0.18001	0.00200	1098	46	1077	16	1067	11	29	78	0.37	99%
91500std	0.07367	0.00181	1.81250	0.04821	0.17833	0.00196	1031	49	1050	17	1058	11	30	80	0.37	99%
GJ-600	0.05793	0.00124	0.78697	0.01804	0.09869	0.00113	528	46	589	10	607	7	16	196	0.08	97%
STS-3-41	0.08508	0.00134	2.84293	0.05640	0.24304	0.00373	1318	30	1367	15	1403	19	97	182	0.53	97%
STS-3-42	0.05800	0.00113	0.68196	0.01437	0.08526	0.00092	528	43	528	9	528	6	481	313	1.54	99%
STS-3-43	0.07073	0.00128	1.51117	0.02811	0.15523	0.00151	950	32	935	11	930	8	107	177	0.61	98%
STS-3-44	0.06888	0.00093	1.36548	0.02007	0.14351	0.00124	894	23	874	9	865	7	26	507	0.05	98%
STS-3-45	0.10551	0.00125	4.60495	0.06599	0.31610	0.00317	1724	22	1750	12	1771	16	38	214	0.18	98%
STS-3-46	0.10823	0.00127	4.69456	0.06341	0.31412	0.00302	1770	21	1766	11	1761	15	88	197	0.45	99%
STS-3-47	0.09808	0.00194	3.79443	0.07295	0.28158	0.00312	1588	37	1592	16	1599	16	88	48	1.83	99%
STS-3-48	0.07580	0.00117	1.85915	0.03091	0.17761	0.00170	1100	31	1067	11	1054	9	94	229	0.41	98%
STS-3-81	0.06171	0.00118	0.84341	0.01874	0.09883	0.00131	665	36	621	10	608	8	77	242	0.32	97%
SRM 610	0.92177	0.01042	28.73780	0.36374	0.22576	0.00221	/	/	3445	13	1312	12	548	542	1.01	10%
91500std	0.07515	0.00148	1.85642	0.03891	0.17926	0.00217	1072	45	1066	14	1063	12	30	79	0.37	99%
91500std	0.07461	0.00148	1.84398	0.03900	0.17908	0.00204	1057	40	1061	14	1062	11	30	80	0.37	99%
GJ-600	0.06019	0.00116	0.81706	0.01750	0.09839	0.00121	609	41	606	10	605	7	16	192	0.08	99%
STS-3-49	0.05793	0.00119	0.67822	0.01478	0.08492	0.00094	528	46	526	9	525	6	382	263	1.45	99%
STS-3-50	0.16373	0.00196	9.84665	0.13007	0.43519	0.00402	2495	19	2421	12	2329	18	74	109	0.68	96%
STS-3-51	0.08084	0.00087	2.26460	0.02803	0.20249	0.00172	1218	21	1201	9	1189	9	184	499	0.37	98%
STS-3-52	0.07217	0.00087	1.66344	0.02546	0.16678	0.00201	991	26	995	10	994	11	337	472	0.71	99%
STS-3-53	0.07240	0.00109	1.59051	0.02571	0.15895	0.00149	998	31	967	10	951	8	27	239	0.11	98%
STS-3-54	0.06103	0.00122	0.84344	0.01632	0.10051	0.00108	639	43	621	9	617	6	125	162	0.77	99%
STS-3-55	0.05851	0.00087	0.68909	0.01118	0.08520	0.00088	550	36	532	7	527	5	326	546	0.60	99%
STS-3-56	0.07155	0.00108	1.58576	0.02562	0.16032	0.00157	973	30	965	10	959	9	116	315	0.37	99%
Ple-337	0.05533	0.00117	0.40980	0.00910	0.05358	0.00056	433	48	349	7	336	3	38	431	0.09	96%
91500std	0.07304	0.00181	1.80685	0.04588	0.17943	0.00210	1017	50	1048	17	1064	11	28	78	0.37	98%
91500std	0.07672	0.00182	1.89355	0.04740	0.17891	0.00235	1114	48	1079	17	1061	13	26	71	0.36	98%
GJ-600	0.06148	0.00130	0.82710	0.01878	0.09726	0.00109	657	46	612	10	598	6	16	192	0.08	97%
STS-3-57	0.07610	0.00108	1.89206	0.02961	0.17976	0.00180	1098	-4	1078	10	1066	10	159	464	0.34	98%
STS-3-58	0.13613	0.00164	7.72937	0.11945	0.40994	0.00453	2189	21	2200	14	2215	21	56	313	0.18	99%
STS-3-59	0.07106	0.00105	1.53577	0.02618	0.15621	0.00163	959	32	945	11	936	9	59	302	0.2	99%
STS-3-60	0.11554	0.00155	5.37681	0.08066	0.33647	0.00316	1888	29	1881	13	1870	15	133	118	1.13	99%

Table 2. *Cont.*

Analysis	$^{207}Pb/^{206}Pb$		$^{207}Pb/^{235}U$		$^{207}Pb/^{238}U$		$^{207}Pb/^{206}Pb$		$^{207}Pb/^{235}U$		$^{206}Pb/^{238}U$		Th	U	Th/U	Concordance
	Ratio	1σ	Ratio	1σ	Ratio	1σ	Age	1σ	Age	1σ	Age	1σ	ppm	ppm		
STS-3-61	0.09935	0.00176	3.78490	0.06998	0.27589	0.00295	1613	33	1590	15	1571	15	57	59	0.96	98%
STS-3-62	0.07390	0.00096	1.69859	0.02752	0.16603	0.00185	1039	26	1008	10	990	10	45	501	0.09	98%
STS-3-63	0.08980	0.00110	3.07350	0.04263	0.24775	0.00249	1421	29	1426	11	1427	13	190	504	0.38	99%
STS-3-64	0.05975	0.00153	0.77524	0.02061	0.09402	0.00101	595	56	583	12	579	6	42	118	0.35	99%
SRM 610	0.92462	0.01208	28.39805	0.40686	0.22214	0.00206	/	/	3433	14	1293	11	548	542	1.01	9%
91500std	0.07480	0.00178	1.84791	0.04625	0.17920	0.00221	1065	48	1063	17	1063	12	26	72	0.36	99%
91500std	0.07496	0.00169	1.85249	0.04512	0.17914	0.00237	1133	50	1064	16	1062	13	29	79	0.37	99%
GJ-600	0.06139	0.00128	0.83010	0.01830	0.09790	0.00105	654	44	614	10	602	6	16	191	0.08	98%
STS-3-65	0.07632	0.00117	2.05412	0.03641	0.19458	0.00204	1103	36	1134	12	1146	11	92	224	0.41	98%
STS-3-66	0.05753	0.00156	0.68101	0.01506	0.08500	0.00086	522	61	527	9	526	5	395	224	1.76	99%
STS-3-67	0.06363	0.00093	1.03389	0.01789	0.11760	0.00135	729	32	721	9	717	8	178	397	0.45	99%
STS-3-68	0.12658	0.00143	6.48720	0.08550	0.37103	0.00362	2051	20	2044	12	2034	17	112	270	0.42	99%
STS-3-69	0.07342	0.00097	1.77024	0.02654	0.17436	0.00156	1026	28	1035	10	1036	9	199	353	0.57	99%
STS-3-70	0.09867	0.00122	3.39063	0.04741	0.24851	0.00212	1599	23	1502	11	1431	11	136	363	0.38	95%
STS-3-71	0.08322	0.00118	2.12369	0.04494	0.18348	0.00250	1276	23	1157	15	1086	14	97	355	0.27	93%
STS-3-72	0.07678	0.00135	1.94578	0.03415	0.18403	0.00180	1117	35	1097	12	1089	10	56	113	0.50	99%
Ple-337	0.05437	0.00095	0.40739	0.00836	0.05423	0.00068	387	44	347	6	340	4	104	816	0.13	98%
91500std	0.07493	0.00177	1.86008	0.04707	0.17979	0.00211	1133	52	1067	17	1066	12	30	81	0.37	99%
91500std	0.07483	0.00165	1.84032	0.04200	0.17855	0.00200	1065	44	1060	15	1059	11	30	81	0.37	99%
GJ-600	0.06163	0.00127	0.83416	0.01806	0.09814	0.00107	661	44	616	10	603	6	16	191	0.08	97%
STS-3-73	0.05828	0.00148	0.68407	0.01736	0.08524	0.00088	539	56	529	10	527	5	193	138	1.40	99%
STS-3-74	0.07818	0.00127	2.08670	0.03757	0.19323	0.00206	1152	31	1144	12	1139	11	125	197	0.64	99%
STS-3-75	0.07357	0.00101	1.69236	0.02649	0.16638	0.00162	1029	23	1006	10	992	9	203	342	0.59	98%
STS-3-76	0.06327	0.00097	0.97519	0.01632	0.11156	0.00106	717	33	691	8	682	6	121	368	0.33	98%
STS-3-77	0.06761	0.00136	1.25360	0.02488	0.13492	0.00153	857	42	825	11	816	9	94	107	0.88	98%
STS-3-78	0.07316	0.00108	1.62807	0.02791	0.16073	0.00160	1018	31	981	11	961	9	144	299	0.48	97%
STS-3-79	0.10025	0.00143	4.03175	0.06710	0.29070	0.00299	1629	27	1641	14	1645	15	114	135	0.84	99%
STS-3-80	0.05835	0.00164	0.74682	0.02007	0.09314	0.00095	543	66	566	12	574	6	46	102	0.46	98%
SRM 610	0.93316	0.01209	28.89784	0.38974	0.22405	0.00200	/	/	3450	13	1303	11	548	542	1.01	9%
91500std	0.07348	0.00172	1.81299	0.04310	0.17893	0.00204	1028	42	1050	16	1061	11	25	69	0.36	98%
91500std	0.07628	0.00172	1.88741	0.04477	0.17941	0.00212	1102	44	1077	16	1064	12	25	70	0.36	98%
GJ-600	0.05983	0.00126	0.80980	0.01706	0.09820	0.00099	598	46	602	10	604	6	16	190	0.08	99%
Ple-337	0.05576	0.00102	0.41598	0.00808	0.05394	0.00054	443	8	353	6	339	3	57	637	0.09	95%

5. Discussion

5.1. Sedimentary Facies Units

Through field observation and identification of rock types and sedimentary structures of the conglomerates that are horizons in the lowest part of the Dongchong Formation in the Shita Mountain section, 12 lithofacies and 5 lithofacies associations were established. The obtained results were compared with the alluvial fan depositional types [30–33], suggesting that the conglomerates in this area are closely related to the shelf-type fan delta, which mainly occurs in debris flow, tractive flow, flood flow, and rock flow.

This study proposes the classification of the conglomerates developed in Shita Mountain as the fan root subfacies of the fan delta. The sedimentary microfacies units can be divided into debris-flow deposits, braided channels, sieve deposits, and sheet-flow deposits. The conglomerate at the bottom of the Dongchong Formation is 18 m thick, which shows a three-part characteristic. The lower unit primarily consists of debris channels and channels, with a thickness of 6 m. The middle unit, which is 8.1 m thick, is composed of braided channels and inter-channel lenticular sandstones, interbedded with sieve deposits and occasionally containing sheet-flow deposits. The upper unit is predominantly deposited by debris flow and has a thickness of 3.9 m. On the whole, these units form an upwardly coarsening progradational sedimentary sequence. It is over-covered by about 9 m thick nearshore facies-retained gravels. The bottom boundary of the conglomerate of the Dongchong Formation is in a minor-angle unconformity contact with the purple-reddish medium-thin fine sandstones of the underlying Luohong Formation. This suggests that the conglomerate formation was primarily influenced by tectonic uplift processes.

5.2. Age of the Conglomerates

In the Shita Mountain section, while no fossils have been discovered within the conglomerate layer, fossils have been documented in the overlying upper layer. In the 1:200,000 Geological Survey Report of Luoding, faunal assemblages were documented in gray-white, fine-grained quartz sandstones interbedded with siltstones above the purplish-

red conglomerate layer of Suweiling (now Shita Mountain). This pioneer work revealed the presence of trilobites, including *Illaenus sinenis*, *I.* sp. and *Synhomalonatus birmanica*, along with brachiopods (*Orthis carausis*, *O. calligramma intercalave*, *O. calligramma hupehensis*, *Metorthis delicata*, and *Martella* cf. *ichangensis*) and gastropod fauna. According to the report, these fossils are commonly found in the Middle Ordovician Aijiashanian Stage of Hubei and Southern Shaanxi along the Yangtze River. The genus and species of the fossils were subsequently referenced by the Central-South China Regional Stratigraphic Time Scale Compilation Group [34] and the Bureau of Geology and Mineral Resources of Guangdong Province [20].

In 2019, our research team conducted a fossil collection campaign in the Shita Mountain area, targeting the medium-coarse-grained sandstone layer located directly above the conglomerate layer at the mountain's summit. Despite the fossils' unsatisfactory state of preservation, they still possess a significant identification value. The fossils were identified as *Syntrophinella* sp. and *Orthambonites* sp., indicative of an early Middle Ordovician age (Figure 6).

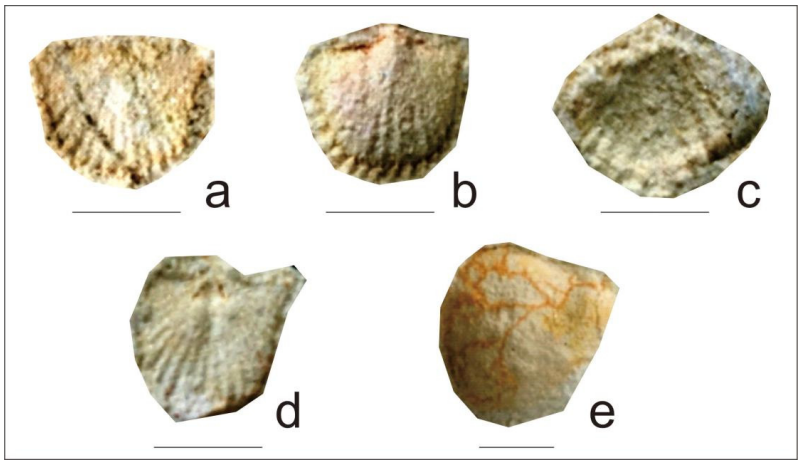


Figure 6. Brachiopod fossils preserved in sandstones at Shita Mountain: (**a**–**d**) *Orthambonites* sp. and (**e**) *Syntrophinella* sp. The scale bar represents 0.5 cm. All fossils are kept in the Wuhan Center, China Geological Survey.

When examining the appearance of the conglomerates at the boundary between the Luohong Formation and the Dongchong Formation, the lithological characteristics change obviously and have a certain spatial distribution, which is beneficial for field work. Wang et al. [17] described a fossil group dominated by trilobites in the Lanweng Formation, which corresponds to the upper part of the section. This fossil group includes species such as *Nankinolithus wanyuanensis*, *N. nankinensis*, *N.* sp., *Dionide* sp., *Ampyx abnormis*, *A.* sp., *Nileus* sp., *Cyclopyge* sp. 1, *C.* sp. 2, *Lisogorites* sp., *Birmanites*? sp., *Ovalocephalus* sp., and *Asaphidae* (gen. et sp. indet.). In addition to these trilobites, brachiopods, echinoderms, and machaeridians are also present, indicating a Late Ordovician age. Based on our findings, we suggest that the deposition of the conglomerate unit predates the fossil-bearing layers, indicating an age slightly earlier than the fossil assemblages. It is hypothesized that the conglomerate unit likely represents a transitional age during the Early–Middle Ordovician period.

5.3. Reconsideration of the Yunan Orogeny

5.3.1. The Conglomerate Difference between Luohong and Dongchong Formations

The type section of the Luohong Formation is located in Luohong Village, Deqing County. The basal conglomerate of the Luohong Formation has been widely recognized as a characteristic feature associated with the Yunan Orogeny, indicating its affiliation with the Lower Ordovician period [11,13,14,23,35,36].

The Luohong Formation's type section exhibits a predominantly coarse clastic rock sequence, characterized by grayish-white and yellowish-white conglomerates, glutenites, pebble-bearing feldspathic quartz sandstones, and pebble-bearing phyllites. The conglomerate layer is primarily concentrated in the lower part of the formation, with sporadic occurrences of gravels observed in the upper sections. The composition of gravels is mostly metamorphic quartz sandstones, with a small number of argillaceous siltstones and siliceous rocks. The particle size of gravels ranges from 1.5 cm to 20 cm, with an average size of 6~7 cm. In particular, the largest flat faces of all pebbles are nearly parallel to the bedding surface. The conglomerate layer is characterized by moderate sorting and rounded to subrounded gravels, representing the primary constituent of the conglomerate.

The conglomerate layer of the Lower Ordovician Luohong Formation is generally considered to have the characteristics of basal conglomerate with significant tectonic movements; however, some scholars have proposed that it is a turbidite fan [37] or a submarine alluvial fan deposit [38].

By conducting a field survey of the type section of the Luohong Formation again, we observed significant weathering, although some gravels remain visible. These gravels have a subrounded to rounded shape and could be divided into matrix-rich conglomerate facies and matrix-poor conglomerate facies from the bottom to the top, showing typical debris-flow characteristics rather than a turbidity flow with positive grading. The sedimentary features resemble those of a main channel within a submarine fan system. Therefore, our findings align with the perspective presented by the Guangdong Geological Survey Institute [38].

In addition, multiple conglomerate layers have been identified in Tongmen town, Deqing County. Through a field geological survey, we observed that the gravels in these layers are well rounded, and the composition is mainly sandstones, which have a well-sorted and certain orientation. The sedimentary characteristics of these conglomerates suggest a depositional environment associated with submarine fan deposits, previously assigned to the Middle Ordovician Dongchong Formation [23]. However, after isotope dating, the granitic pebbles found within the sandstones yielded an age range of 430–420 Ma, indicating a Silurian age for the deposits (unpublished data).

In general, the gravel characteristics of the Early Ordovician Luohong Formation's type section in Luohong Village, Deqing, differ from the Middle Ordovician Dongchong Formation on the Shita Mountain. Previously, these two conglomerate layers were regarded as the stratigraphic horizon markers of the Yunan Orogeny at the transition period from Cambrian to Ordovician. However, the current evidence shows that the difference between them is not only in age, but also in geological and scientific significance.

5.3.2. Two Episodes of Yunan Orogeny

The Yunan Orogeny is a tectonic movement that occurred between the Pan-African collisional orogeny and the breakup of the Gondwana continent. It was equivalent to a small number of metamorphic events between 520 and 470 Ma [36,39] and synchronized with the widespread orogenic event in the northern margin of East Gondwana. Nevertheless, South China occupied a position toward the terminal region of the collision zone, resulting in minimal influence and limited occurrences of coeval magmatism and metamorphism [16]. The Yunan orogeny has been attributed to the far-field stress induced by the collision between South China and Indian Gondwana [40]. In South China, the effects of this tectonic event are relatively mild and are represented by a local disconformity at the base of the Ordovician succession, but elsewhere in north Gondwana, they are marked by an angular unconformity with a metamorphism of older units and relatively widespread magmatic activity [11]. According to the records of Guangdong Lithostratigraphy [41], the thickness of the conglomerate-concentrated layer in the type section of the Luohong Formation is about 35 m. The discovery of important Early Ordovician graptolite fossils, such as Anisograptus and Bryograptus, in the shale above the conglomerate layer further confirms the geological age of the conglomerate layer [42].

The distinct sedimentary successions observed in the concentrated layers of the Luohong and Dongchong Formations reflect two different episodes of the Yunan Orogeny, which were possibly driven by tectonic activities. The first episode of the Yunan Orogeny refers to the tectonic movement corresponding to the conglomerate layer at the base of the Luohong Formation in the Early Ordovician. There are two types of Ordovician sediments in Guangdong Province: one is graptolite shale and clastic facies, represented by Liuchen in Guangxi, Taishan and Shaoguan in Guangdong, and the other is flysch neritic clastic facies represented by the Yunkai area [20]. The former has a conformable contact between the Cambrian and Ordovician secession, such as the Shenjing section in Taishan, the Laoshuzhai section in Qujiang, and the Yangmeidong section in Nanxiong, showing the differences in lithology caused by a change in sea level. The latter is represented by the type section of the Luohong Formation in Deqing. The study conducted by Nan and Zhou [41] initially suggested an unconformity between the Luohong Formation and the underlying Cambrian strata. However, our findings indicate that the gravel layer in the study area was actually a result of submarine fan deposits rather than uplift and exposure. This deposition could be attributed to the steepening of the paleotopography of the seafloor. In other words, the first episode of the Yunan Orogeny in the Yunkai area was characterized by changes in seafloor topography, without evident exposure or fold deformation.

During the Early–Middle Ordovician transition, the conglomerate layer found at the base of the Dongchong Formation represents the second episode of the Yunan Orogeny. The sedimentary microfacies units of the Shita Mountain fan-toe subfacies can be divided into debris-flow deposits, braided channels, sieved sediment, debris channels, and a small amount of sheet-flow deposits. In the lower part of the Dongchong Formation, debris channels and inter-channel deposits dominate, while the middle part is characterized by braided channels with lens-shaped sandstones intercalated with sieved sediments, occasionally accompanied by a very small amount of sheet-flow deposits. The upper part is predominantly composed of debris-flow deposits, forming an upward coarsening progradational sedimentary sequence. Overlying these deposits is a nearshore facies with a lag gravel layer, which we speculate to be the result of local tectonic uplift acting as a base-level change. This sedimentary response is characterized by the presence of purple-reddish polymictic conglomerates, which can be correlated with Beds 8–10 in the Shita Mountain section. The notable similarities in lithological attributes, sedimentary facies, and stratigraphic positioning substantiate their correlation and reinforce the inference that these conglomerates represent exposed sedimentary units. These conglomerates document the transition from an exposed surface to an alluvial fan and coastal facies, indicating a gradual deepening of seawater. Furthermore, a distinct parallel unconformity is observed between the Dongchong Formation and the underlying Luohong Formation. There exists a temporal gap between the first episode and the second episode of the Yunan Orogeny, representing a relatively continuous process. However, the second episode exhibits more prominent characteristics compared to the first episode.

5.3.3. Regional Comparison of the Yunan Orogeny

Cawood et al. [5] inferred that the location of the SCB was at the nexus between Western Australia and northern India because of their high similarity in stratigraphic sequence and detrital-zircon age spectra. Xu et al. [9] suggested that the SCB constituted part of the lithosphere of greater India and was separated from Australia by the Kuunga Ocean. Due to the collision between the SCB and Western Australia, an unconformity surface between the Cambrian and Ordovician secession that was widely distributed in the northern margin of East Gondwana was formed, and it was displayed as the Yunan Orogeny in the Cathysian and the south-west tectonic structure at the southern margin of the SCB. Most of the previous studies focused on the first episode of the Yunan Orogeny at the transition of the Cambrian–Ordovician boundary. Qin et al. [43] showed that the lower Ordovician Liuchen Formation and the underlying Cambrian Huangdongkou Formation were in a parallel unconformity contact in Malu, Cenxi City, on the west margin of Yunkai,

with conglomerates, gravel-bearing sandstones, and local 1–3 cm iron shells at the bottom. The sedimentary response of the Yunan Orogeny in the Sanya area of Hainan Island might be a parallel unconformity contact between the Middle Cambrian Damao Group and the Upper Cambrian Dakui Group [44]. Zhang et al. [36] suggested that the 490 Ma magmatism in the Wuping area might be correlated with the Yunan Orogeny (our first episode), representing a rapid tectonic uplifting event. However, according to the evidence we have so far, at least in western Guangdong, this tectonic activity was not so strong, and it only manifested as changes in seabed paleotopography and a differentiation of sedimentary facies, forming a sedimentary record of submarine fans.

The second episode of the Yunan Orogeny (ca., 470 Ma) is related to the continuous effects of the plate–margin collision at the turn of the Cambrian–Ordovician and the intracontinental orogeny widely distributed in the northern margin of Gondwana, and it is the continuation of the first episode, with a short interval between them. Conglomerates from the basal Dongchong Formation were found nearby in Lanzhai, Nanjiangkou [23]. Nevertheless, pebble-bearing, medium-coarse sandstones above the limestone layer of the Luodong Formation in Yuecheng were also found in Gaoyao, Guangdong, which belongs to the Dongchong Formation as well [41]. The conglomerate layer at the top of Shita Mountain was not well discovered via lateral tracing, because Ordovician (actually the entire pre-Devonian succession) fossils in the Yunkai area were scarce in the past. It is very difficult to obtain evidence that can determine the age of strata in clastic rocks. The previous understanding that the conglomerates in Tongmen belonged to the Dongchong Formation had been challenged by subsequent zircon dating of granitic gravels, which does not support this interpretation. The Qianzhong uplift within the Yangtze block is regarded as one of the manifestations of the Yunan Orogeny [45]. The second episode of this orogenic event might have continued to uplift on the basis of the first episode, resulting in a sedimentary discontinuity between the Lower and Middle Ordovician [46]. The northwestern Shaowu–Taining area in Fujian lacks Middle Ordovician sediments, which might possess the same structural characteristics as those in the Middle Ordovician area [47].

As previously discussed, it is postulated that the Yunan Orogeny was likely primarily driven by the collision between the SCB and Western Australia during the Cambrian–Ordovician period. This collision is believed to have exerted a significant influence, undergoing at least two distinct tectonic events of varying intensity during the Late Cambrian and Early–Middle Ordovician. Importantly, the timing of the second tectonic event aligned with the recognized Bhimphedian Orogeny in the northern Indian region [6], further supporting the hypothesis.

5.3.4. Probable Provenance based on Detrital Zircon U-Pb Ages

The Shita Mountain is located on the western side of the Cathaysia Block, and therefore its sediments are believed to have primarily originated from the Ross–Delamerian Orogen, Wilkes–Albany–Fraser Belt, and Western Australia [48]. The detrital zircon LA-ICP-MS U-Pb ages obtained from the Dongchong Formation indicate the influence of multiple tectonothermal events on the source area, supporting the findings of previous investigations in the adjacent regions. The detrital zircon grains exhibit a broad distribution of U-Pb ages, characterized by prominent age clusters at 522~628 Ma, 930~1103 Ma, and 1421~1750 Ma (Table 2). The U-Pb ages obtained from dating detrital zircons within the sediments of Shita Mountain were compared with previously reported zircon U-Pb ages from diverse sources reported by different researchers to infer the provenance of the studied sediments (Figure 7).

The age distributions observed in this study for detrital zircons have also been documented in sediments from the northern margin of Gondwana [4,49–56]. The obtained results indicate that a wide-ranging source area contributed a significant quantity of detrital materials to this area. Therefore, in the Yunkai area, the detrital-zircon age spectra from

the Ordovician samples show a strong similarity with India, Antarctica, the Lhasa, the Himalayas, Southern Qiangtang, and Western Australia (Figure 8).

In this study, a prominent age peak at 520~530 Ma is found in the Early–Middle Ordovician of western Guangdong. However, this result has only previously been described in the Cambrian of Northern Guangdong [57] and Southern Hunan [58], and the Ordovician of Eastern Guangxi [59] in the adjacent area. There is a soaring number of detrital zircons of 525–520 Ma in the lower Cambrian in western SCB, which has been interpreted as showing a magmatic arc of similar ages [60]. One potential origin for the 520~530 Ma detrital zircons found in the Shita Mountain samples is the local recycling of Cambrian strata within western SCB, followed by transportation during the Early Ordovician period. In contrast to the reported Cambrian samples, the Shita Mountain samples do not exhibit a prominent peak in the 750~850 Ma range. These results provide further support for the hypothesis, suggesting global plate re-organization at, ca., 520~530 Ma during the Gondwana assembly [61].

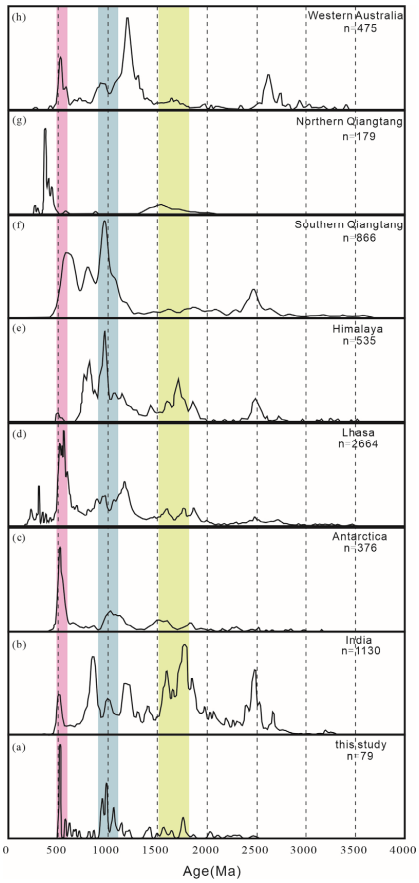


Figure 7. Density probability diagrams of detrital zircons with age histograms representative for (**a**) this study, (**b**) India, (**c**) Antarctica, (**d**) the Lhasa, (**e**) the Himalayas, (**f**) Southern Qiangtang, (**g**) Northern Qiangtang, and (**h**) Western Australia. The age data were compiled from Turner et al. [62], Bickford et al. [63], Malone et al. [64], and Collins et al. [65] for India; Goodge et al. [66] for Antarctica; Gehrels et al. [67], Leier et al. [68], Li et al. [52], Li et al. [69], Pullen et al. [70], and Zhu et al. [56] for the Lhasa; Myrow et al. [54,71], McKenzie et al. [72], and Hughes et al. [73] for the Himalayas; Xu et al. [74] for Southern Qiangtang; Zhang et al. [75] for the Northern Qiangtang; and Cawood and Nemchin [49] and Veevers et al. [76] for Western Australia.

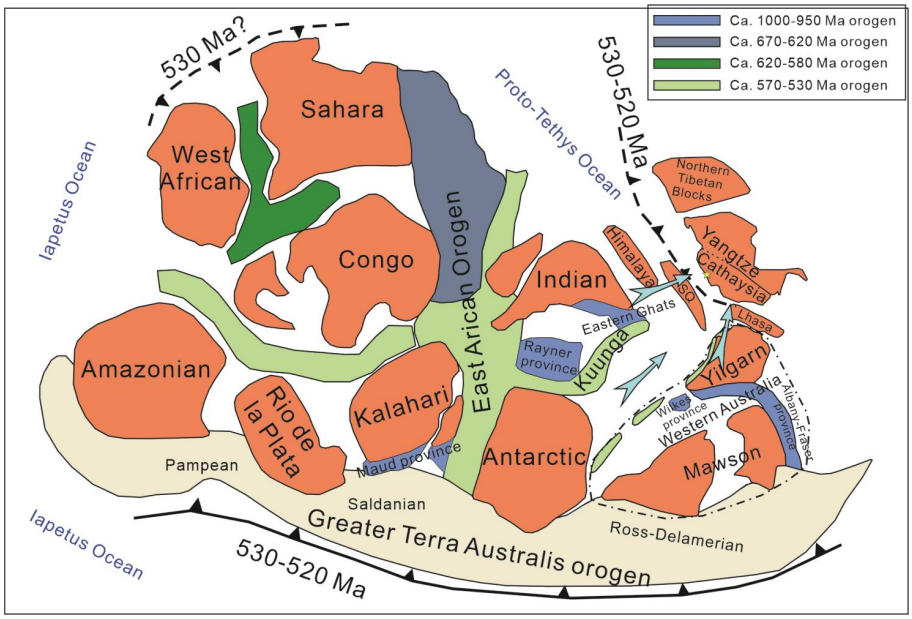


Figure 8. Simplified paleogeographic reconstruction of eastern Gondwana during the Early–Middle Ordovician period (modified after [61,77]). The canal blue arrows indicate possible detritus transport pathways (SQ = Southern Qiangtang). The yellow pentagram represents the study area.

6. Conclusions

Investigation of the Yunkai area in the Early Paleozoic period provides evidence of a two-episode Yunan orogenic event occurring near the Cambrian–Ordovician and Early–Middle Ordovician boundaries, respectively. Twelve lithofacies and five lithological associations were identified based on the conglomerate sequence at the bottom of the Dongchong Formation in the Shita Mountain section, with the age constraints of brachiopod fossils, which support the above viewpoint. The first episode of the Yunan Orogeny resulted in changes in the paleotopography of the seafloor in the Yunkai area, leading to the deposition of a submarine fan conglomerate layer. The second episode was more intense, causing a brief period of exposure and the formation of a sedimentary gap. The dynamic mechanism of the Yunan Orogeny is mainly controlled by the amalgamation of Gondwana. The first episode of the orogeny was synchronous with the widespread orogenic events along the northern margin of East Gondwana. The second episode corresponded to the concluding phase of the North Indian orogeny. The Yunkai area had its provenance from India, Antarctica, the Lhasa, the Himalayas, Southern Qiangtang, and Western Australia. This interpretation sheds new light on the Yunan Orogeny, but further sedimentological investigations of coeval sequences in adjacent regions are necessary to validate this hypothesis on a larger scale and to reconstruct the paleogeography of the Cathaysia Block at the onset of the Phanerozoic era.

Author Contributions: Z.W., Z.L. and Z.N. contributed to the conception and design of the study. Z.W. and Z.L. wrote the first draft of the manuscript. C.L., H.C., X.L. and K.H. participated in the field investigation and sample collection. H.Y. contributed to the data discussion. All authors have read and agreed to the published version of the manuscript.

Funding: This study was supported by the National Natural Science Foundation of China (Nos. 41802018 and 41772019); Key Laboratory of Stratigraphy and Palaeontology, Ministry of Natural Resources (KLSP2105); Hubei Key Laboratory of Paleontology and Geological Environment Evolution (PEL-202006); and Wuhan Center, China Geological Survey (QL2022-07).

Data Availability Statement: The raw data supporting the conclusion of this article will be made available by the authors, without undue reservation.

Acknowledgments: The authors want to express their gratitude to Qingluan Zeng (Wuhan) and Yuchen Zhang (Nanjing) for their invaluable assistance with the identification of brachiopod fossils in this study. Special thanks to Song Fang, Yang Wenqiang, and He Yaoyan (Wuhan) for their support during field work. The first author also acknowledges China Scholarship Council (Grant No. 202108575015) for supporting his research in the University of Münster. We thank four anonymous reviewers, and editors for their comments that led to significant improvements in the manuscript.

Conflicts of Interest: The authors declare that the research was conducted in the absence of any commercial or financial relationships that could be construed as a potential conflict of interest.

References

1. Cawood, P.A.; Zhao, G.C.; Yao, J.L.; Wang, W.; Xu, Y.J.; Wang, Y.J. Reconstructing South China in Phanerozoic and Precambrian supercontinents. *Earth Sci. Rev.* **2018**, *186*, 173–194. [CrossRef]
2. Li, Z.X.; Li, X.H.; Zhou, H.W.; Kinny, P.D. Grenvillian continental collision in south China: New SHRIMP U-Pb zircon results and implications for the configuration of Rodinia. *Geology* **2002**, *30*, 163–166. [CrossRef]
3. Li, W.; Li, X.; Li, Z. Neoproterozoic bimodal magmatism in the Cathaysia Block of South China and its tectonic significance. *Precambrian Res.* **2005**, *136*, 51–66. [CrossRef]
4. Wang, Y.J.; Fan, W.M.; Zhang, G.W.; Zhang, Y.H. Phanerozoic tectonics of the South China Block: Key observations and controversies. *Gondwana Res.* **2013**, *23*, 1273–1305. [CrossRef]
5. Cawood, P.A.; Wang, Y.J.; Xu, Y.J.; Zhao, G.C. Locating South China in Rodinia and Gondwana: A fragment of greater India lithosphere? *Geology* **2013**, *41*, 903–906. [CrossRef]
6. Cawood, P.A.; Johnson, M.R.W.; Nemchin, A.A. Early palaeozoic orogenesis along the Indian margin of Gondwana: Tectonic response to Gondwana assembly. *Earth Planet. Sci. Lett.* **2007**, *255*, 70–84. [CrossRef]
7. Cawood, P.A.; Martin, E.L.; Murphy, J.B.; Pisarevsky, S.A. Gondwana's interlinked peripheral orogens. *Earth Planet. Sci. Lett.* **2021**, *568*, 117057. [CrossRef]
8. Wang, Z.H.; Yang, W.Q.; Zhou, D.; Niu, Z.J.; He, Y.Y.; Song, F. Detrital zircon U-Pb geochronological records and its response of provenance transformation of strata surrounding Cambrian-Devonian unconformity in Eastern margin of Yunkai Massif. *Earth Sci.* **2018**, *43*, 4193–4203, (In Chinese with English abstract)
9. Xu, Y.J.; Cawood, P.A.; Du, Y.S. Intraplate Orogenesis in Response to Gondwana Assembly: Kwangsian Orogeny, South China. *Am. J. Sci.* **2016**, *316*, 329–362. [CrossRef]
10. Xu, Y.J.; Cawood, P.A.; Du, Y.S.; Hu, L.S.; Yu, W.C.; Zhu, Y.H.; Li, W.C. Linking south China to northern Australia and India on the margin of Gondwana: Constraints from detrital zircon U-Pb and Hf isotopes in Cambrian strata. *Tectonics* **2013**, *32*, 1547–1558. [CrossRef]
11. Xu, Y.J.; Cawood, P.A.; Du, Y.S.; Huang, H.W.; Wang, X.Y. Early Paleozoic orogenesis along Gondwana's northern margin constrained by provenance data from South China. *Tectonophysics* **2014**, *636*, 40–51. [CrossRef]
12. Niu, Z.J.; Wang, Z.H.; Zhang, R.J.; Lin, X.M.; Li, C.A.; Yang, W.Q.; Yan, C.W.; He, Y.Y.; Song, F. A preliminary study on Middle Ordovician bivalves from Yunkai Area, Western Guangdong, South China. *Earth Sci.* **2018**, *43*, 2195–2205. [CrossRef]
13. Mo, Z.S.; Ye, B.D.; Pan, W.Z. *Granite Geology of Nanling*; Geological Publishing House: Beijing, China, 1980; pp. 4–7. (In Chinese)
14. Qiu, Y.X. Regional tectonic evolution and its basic features in Guangdong province. *Guangdong Geol.* **1992**, *7*, 1–26, (In Chinese with English abstract)
15. Wu, H.R. Reinterpretation of the Guangxi Orogeny. *Chin. Sci. Bull.* **2000**, *45*, 1244–1248, (In Chinese with English abstract)
16. Xu, Y.J.; Du, Y.S. From periphery collision to intraplate orogeny: Early Paleozoic Orogenesis in Southeastern part of South China. *Earth Sci.* **2018**, *43*, 333–353, (In Chinese with English abstract)
17. Wang, Z.H.; Zong, R.W.; Niu, Z.J.; Lin, X.M.; Li, C.A.; Yan, C.W.; Song, F.; He, Y.Y. Discovery of Late Ordovician fossils and its geological significance in Deqing, Western Guang. *J. Stratigr.* **2019**, *43*, 1–8, (In Chinese with English abstract)
18. Zhao, G.; Cawood, P.A. Tectonothermal evolution of the Mayuan Assemblage in the Cathaysia Block; implications for Neoproterozoic collision-related assembly of the South China Craton. *Am. J. Sci.* **1999**, *299*, 309–339. [CrossRef]
19. Zhao, J.H.; Zhou, M.F.; Yan, D.P.; Zheng, J.P.; Li, J.W. Reappraisal of the ages of Neoproterozoic strata in South China: No connection with the Grenvillian orogeny. *Geology* **2011**, *39*, 299–302. [CrossRef]
20. Bureau of Geology and Mineral Resources of Guangdong Province (BGMRGP). *Regional Geology of the Guangdong Province*; Geological Publishing House: Beijing, China, 1988; pp. 1–941, (In Chinese with English abstract)
21. Wang, Y.J.; Zhang, F.F.; Fan, W.M.; Zhang, G.W.; Chen, S.Y.; Cawood, P.A.; Zhang, A.M. Tectonic setting of the South China Block in the early Paleozoic: Resolving intracontinental and ocean closure models from detrital zircon U-Pb geochronology. *Tectonics* **2010**, *29*, TC6020. [CrossRef]
22. Xue, E.K.; Wang, W.; Zhou, M.F.; Pandit, M.K.; Huang, S.F.; Lu, G.M. Late Neoproterozoic–early Paleozoic basin evolution in the Cathaysia Block, South China: Implications of spatio-temporal provenance changes on the paleogeographic reconstructions in supercontinent cycles. *Geol. Soc. Am. Bull.* **2021**, *133*, 717–739. [CrossRef]

23. Xu, H.S.; Yan, C.W.; Li, C.A.; Lin, X.M.; Niu, Z.J.; Zhang, X.H.; Xu, G.J.; Wang, Z.H. The sedimentary sequence and fossil record of Ordovician in Yunan and Deqing Regions, Western Guangdong, South China. *Geol. Miner. Resour. South China* **2017**, *33*, 207–214, (In Chinese with English abstract)
24. Zhang, R.J.; Niu, Z.J.; Li, C.A.; Wang, Z.H.; Song, F.; He, Y.Y.; Yang, W.Q.; Lin, X.M. Yunannioidea—A new superfamily of Pteriomorphids (Bivalvia) from the Middle Ordovician, Yunkai area, western Guangdong, South China. *Acta Palaeontol. Sin.* **2021**, *60*, 357–375, (In Chinese with English abstract)
25. Miall, A.D. Lithofacies types and vertical profile models in braided river deposits: A summary. *Flvial Sedimentol.* **1977**, *5*, 597–604.
26. Miall, A.D. A review of the braided-river depositional environment. *Earth-Sci. Rev.* **1977**, *13*, 1–62. [CrossRef]
27. Thompson, J.M.; Meffre, S.; Danyushevsky, L. Impact of air, laser pulse width and fluence on U-Pb dating of zircons by LA-ICPMS. *J. Anal. At. Spectrom.* **2018**, *33*, 221–230. [CrossRef]
28. Paton, C.; Woodhead, J.D.; Hellstrom, J.C.; Hergt, J.M.; Greig, A.; Maas, R. Improved laser ablation U-Pb zircon geochronology through robust downhole fractionation correction. *Geochem. Geophys. Geosystems* **2010**, *11*, Q0AA06. [CrossRef]
29. Sircombe, K.N. Tracing provenance through the isotope ages of littoral and sedimentary detrital zircon, eastern Australia. *Sediment. Geol.* **1999**, *124*, 47–67. [CrossRef]
30. Bull, W.B. The alluvial-fan environment. *Prog. Phys. Geogr. Earth Environ.* **1977**, *1*, 222–270. [CrossRef]
31. DeCelles, P.G.; Gray, M.B.; Ridgway, K.D.; Cole, R.B.; Pivnik, D.A.; Pequera, N.; Srivastava, P. Controls on synorogenic alluvial-fan architecture, Beartooth Conglomerate (Palaeocene), Wyoming and Montana. *Sedimentology* **1991**, *38*, 567–590. [CrossRef]
32. Garzanti, E.; Casnedi, R.; Jadoul, F. Sedimentary Evidence of a Cambro-Ordovician Orogenic Event in the Northwestern Himalaya. *Sediment. Geol.* **1986**, *48*, 237–265. [CrossRef]
33. Yu, X.H.; Qu, J.H.; Tan, C.P.; Zhang, L.; Li, X.L.; Gao, Z.P. Conglomerate lithofacies and origin models of fan deltas of Baikouquan Formation in Mahu sag, Junggar basin. *Xinjiang Pet. Geol.* **2014**, *35*, 619–627, (In Chinese with English abstract)
34. Central-South China Regional Stratigraphic Time Scale Compilation Group. *Regional Stratigraphic Time Scale of Central-South China*; Geological Publishing House: Beijing, China, 1974. (In Chinese)
35. Du, Y.S.; Xu, Y.J. A preliminary study on Caledonian Event in South China. *Geol. Sci. Technol. Inf.* **2012**, *31*, 43–49, (In Chinese with English abstract)
36. Zhang, A.M.; Wang, Y.J.; Fan, W.M.; Zhang, F.F.; Zhang, Y.Z. LA-ICPMS Zircon U-Pb Geochronology and Hf Isotopic Composition of the Taoxi Migmatite (Wuping): Constrainson the Formation Age of the Taoxi Complex and the Yu'nanian Event. *Geotecton. Metallog.* **2011**, *35*, 64–72, (In Chinese with English abstract)
37. Liu, B.J.; Xu, X.S.; Pan, X.N.; Huang, H.Q.; Xu, Q. *The Sedimentary Crust Evolution and Mineralization of Paleocontinent in Southern China*; Science Press: Beijing, China, 1993. (In Chinese)
38. Guangdong Geological Survey Institute. *Regional Geology of China, Guangdong Province*; Geological Publishing House: Beijing, China, 2021. (In Chinese)
39. Yu, J.H.; Wang, L.J.; Wei, Z.Y.; Sun, T.; Shu, L.L. Phanerozoic Metamorphic Episodesand Characteristics of Cathaysia Block. *Geol. J. China Univ.* **2007**, *13*, 474–483, (In Chinese with English abstract)
40. Yao, W.H.; Li, Z.X. Tectonostratigraphic history of the Ediacaran–Silurian Nanhua foreland basin in South China. *Tectonophysics* **2016**, *674*, 31–51. [CrossRef]
41. Nan, Y.; Zhou, G.Q. *Guangdong Lithostratigrphy*; China Geosciences University Press: Wuhan, China, 1996. (In Chinese)
42. Bureau of Geology and Mineral Resources of Guangxi Zhuang Autonomous Region (BGMRGZAR). *Regional Geology of the Guangxi Zhuang Autonomous Region*; Geological Publishing House: Beijing, China, 1985. (In Chinese)
43. Qin, X.F.; Li, J.; Li, R.S.; Zhou, F.S.; Hu, G.A.; Li, G.J.; Zhou, K.H.; Xie, L.F.; Pan, Y.W. *Geological Evolution of Bobai-Cenxi Orogenic Belt in the North Margin of Yunkai Block, Southeastern Guangxi*; China Land Press: Beijing, China, 2008; pp. 1–152. (In Chinese)
44. Wang, X.F.; Ma, D.Q.; Jiang, D.H. *Geology of Hainan Island, China, (1st) Stratigraphy and Paleontology*; Geological Publishing House: Beijing, China, 1992. (In Chinese)
45. Deng, X.; Yang, K.G.; Liu, P.L.; She, Z.B. Characteristics and tectonic evolution of Qianzhong Uplift. *Earth Sci. Front.* **2010**, *17*, 79–89, (In Chinese with English abstract)
46. Dai, X.C.; Huang, Y.Z. On the central Guizhou uplift and the isostatic subsidence in the process of its formation. *J. Guizhou Univ. Technol.* **1998**, *27*, 23–26, (In Chinese with English abstract)
47. Fujian Bureau of Geology and Mineral Resources. *Regional Geology of Fujian Province*; Geologcal Publish House: Beijing, China, 1985; pp. 1–671. (In Chinese)
48. Luo, L.; Zeng, L.; Wang, K.; Yu, X.; Li, Y.; Zhu, C.; Liu, S. Provenance investigation for the Cambrian–Ordovician strata from the northern margin of the western Yangtze Block: Implications for locating the South China Block in Gondwana. *Geol. Mag.* **2020**, *157*, 551–572.
49. Cawood, P.A.; Nemchin, A.A. Provenance record of a rift basin: U/Pb ages of detrital zircons from the Perth Basin, Western Australia. *Sediment. Geol.* **2000**, *134*, 209–234. [CrossRef]
50. Gehrels, G.E.; DeCelles, P.G.; Ojha, T.P.; Upreti, B.N. Geologic and U–Th–Pb geochronologic evidence for early Paleozoic tectonism in the Kathmandu thrust sheet, central Nepal Himalaya. *Geol. Soc. Am. Bull.* **2006**, *118*, 185–198. [CrossRef]
51. Gehrels, G.E.; DeCelles, P.G.; Ojha, T.P.; Upreti, B.N. Geologic and U–Pb geochronologic evidence for early Paleozoic tectonism in the Dadeldhura thrust sheet, far-west Nepal Himalaya. *J. Asian Earth Sci.* **2006**, *28*, 385–408. [CrossRef]

52. Li, G.W.; Liu, X.H.; Pullen, A.; Wei, L.J.; Liu, X.B.; Huang, F.X.; Zhou, X.J. In-situ detrital zircon geochronology and Hf isotopic analyses from Upper Triassic Tethys sequence strata. *Earth Planet. Sci. Lett.* **2010**, *297*, 461–470. [CrossRef]
53. Metcalfe, I. Gondwana dispersion and Asian accretion: Tectonic and palaeogeographic evolution of eastern Tethys. *J. Asian Earth Sci.* **2013**, *66*, 1–33. [CrossRef]
54. Myrow, P.M.; Hughes, N.C.; Goodge, J.W.; Fanning, C.M.; Williams, I.S.; Peng, S.C.; Bhargava, O.N.; Parcha, S.K.; Pogue, K.R. Extraordinary transport and mixing of sediment across Himalayan centralGondwana during the Cambrian–Ordovician. *Geol. Soc. Am. Bull.* **2010**, *122*, 1660–1670. [CrossRef]
55. Zhao, Z.B.; Bons, P.D.; Wang, G.H.; Liu, Y.; Zheng, Y.L. Origin and pre-Cenozoic evolution of the south Qiangtang basement, Central Tibet. *Tectonophysics* **2014**, *623*, 52–66. [CrossRef]
56. Zhu, D.C.; Zhao, Z.D.; Niu, Y.L.; Dilek, Y.; Mo, X.X. Lhasa terrane in southern Tibet came from Australia. *Geology* **2011**, *39*, 727–730. [CrossRef]
57. Yao, W.H.; Li, Z.X.; Li, W.X.; Li, X.H.; Yang, J.H. From Rodinia to Gondwanaland: A Tale of Detrital Zircon Provenance Analyses from the Southern Nanhua Basin, South China. *Am. J. Sci.* **2014**, *314*, 278–313. [CrossRef]
58. Yao, W.H.; Li, Z.X.; Li, W.X. Was there a Cambrian ocean in South China?—Insight from detrital provenance analyses. *Geol. Mag.* **2014**, *152*, 184–191. [CrossRef]
59. Yao, W.H.; Li, Z.X.; Li, W.X.; Su, L.; Yang, J.H. Detrital provenance evolution of the Ediacaran–Silurian Nanhua foreland basin, South China. *Gondwana Res.* **2015**, *28*, 1449–1465. [CrossRef]
60. Yang, C.; Li, X.H.; Li, Z.X.; Zhu, M.; Lu, K. Provenance Evolution of Age-Calibrated Strata Reveals When and How South China Block Collided with Gondwana. *Geophys. Res. Lett.* **2020**, *47*, e2020GL090282. [CrossRef]
61. Yao, J.; Cawood, P.A.; Zhao, G.; Han, Y.; Xia, X.; Liu, Q.; Wang, P. Mariana-type ophiolites constrain the establishment of modern plate tectonic regime during Gondwana assembly. *Nat. Commun.* **2021**, *12*, 4189. [CrossRef]
62. Turner, C.C.; Meet, J.G.; Pandit, M.K.; Kamenov, G.D. A detrital zircon U–Pb and Hf isotopic transect across the Son Valley sector of the Vindhyan Basin, India: Implications for basin evolution and paleogeography. *Gondwana Res.* **2014**, *26*, 348–364. [CrossRef]
63. Bickford, M.E.; Basu, A.; Patranabis-Des, S.; Dhang, P.C.; Schieber, J. Depositional history of the Chhattisgarh Basin, Central India: Constraints from new SHRIMP zircon ages. *J. Geol.* **2011**, *119*, 33–50. [CrossRef]
64. Malone, S.J.; Meert, J.G.; Banerjee, D.M.; Pandit, M.K.; Tamrat, E.; Kamenov, G.D.; Pradhan, V.R.; Sohl, L.E. Paleomagnetism and detrital zircon geochronology of the Upper Vindhyan Sequence, Son Valley and Rajasthan, India: A ca. 1000 Ma closure age for the Purana Basins? *Precambrian Res.* **2008**, *164*, 137–159. [CrossRef]
65. Collins, A.S.; Santosh, M.; Braun, I.; Clark, C. Age and sedimentary provenance of the Southern Granulites, South India: U–Th–Pb SHRIMP secondary ion mass spectrometry. *Precambrian Res.* **2007**, *155*, 125–138. [CrossRef]
66. Goodge, J.W.; Williams, I.S.; Myrow, P. Provenance of Neoproterozoic and lower Paleozoic siliciclastic rocks of the central Ross orogen, Antarctica: Detrital record of rift-, passive-, and active-margin sedimentation. *Geol. Soc. Am. Bull.* **2004**, *116*, 1253–1279. [CrossRef]
67. Gehrels, G.E.; Kapp, P.; DeCelles, P.G.; Pullen, A.; Blakey, R.; Weislogel, A.; Ding, L.; Guynn, J.; Martin, A.; McQuarrie, N.; et al. Detrital zircon geochronology of pre-Tertiary strata in the Tibetan-Himalayan orogen. *Tectonics* **2011**, *30*, TC5016. [CrossRef]
68. Leier, A.L.; Kapp, P.; Gehrels, G.E.; DeCelles, P.G. Detrital zircon geochronology of carboniferous-cretaceous strata in the lhasa terrane, Southern Tibet. *Basin Res.* **2007**, *19*, 361–378. [CrossRef]
69. Li, G.; Sandiford, M.; Liu, X.; Xu, Z.; Wei, L.; Li, H. Provenance of Late Triassic sediments in central Lhasa terrane, Tibet and its implication. *Gondwana Res.* **2014**, *25*, 1680–1689. [CrossRef]
70. Pullen, A.; Kapp, P.; Gehrels, G.E.; Vervoort, J.D.; Ding, L. Triassic continental subduction in central Tibet and Mediterranean-style closure of the Paleo-Tethys Ocean. *Geology* **2008**, *36*, 351–354. [CrossRef]
71. Myrow, P.M.; Hughes, N.C.; Searle, M.P.; Fanning, C.M.; Peng, S.C.; Parcha, S.K. Stratigraphic correlation of Cambrian–Ordoviciandeposits along the Himalaya: Implications for the age and nature of rocksin the Mt. Everest region. *Geol. Soc. Am. Bull.* **2009**, *121*, 323–332. [CrossRef]
72. McKenzie, N.R.; Hughes, N.C.; Myrow, P.M.; Xiao, S.; Sharma, M. Correlation of Precambrian–Cambrian sedimentary successions across northern India and the utility of isotopic signatures of Himalayan lithotectonic zones. *Earth Planet. Sci. Lett.* **2011**, *312*, 471–483. [CrossRef]
73. Hughes, N.C.; Myrow, P.M.; McKenzie, N.R.; Harper, D.A.T.; Bhargava, O.N.; Tangri, S.K.; Ghalley, K.S.; Fanning, C.M. Cambrian rocks and faunas of the Wachi La, Black Mountains, Bhutan. *Geol. Mag.* **2011**, *148*, 351–379. [CrossRef]
74. Xu, W.; Zhang, W.; Liu, F.L. Detrital zircon populations of the South Qiangtang terrane, central Tibetan Plateau, and their implications for Tethyan evolution. *Int. Geol. Rev.* **2023**, *65*, 1696–1718. [CrossRef]
75. Zhang, Y.X.; Zheng, B.; Wang, J.; Fu, X.G. Locating northern Qiangtang on the margin of Gondwana or Laurasia? Evidence from detrital zircon geochronology. *J. Asian Earth Sci.* **2022**, *237*, 105343. [CrossRef]

76. Veevers, J.J.; Saeed, A.; Belousova, E.A.; Griffin, W.L. U–Pb ages and source composition by Hf-isotope and trace-element analysis of detrital zircons in Permian sandstone and modern sand from southwestern Australia and a review of the paleogeographical and denudational history of the Yilgarn Craton. *Earth Sci. Rev.* **2005**, *68*, 245–279. [CrossRef]
77. Sun, J.P.; Dong, Y.P.; Jiang, W.; Ma, L.C.; Chen, S.Y.; Du, J.J.; Peng, Y. Reconstructing the Olongbuluke Terrane (northern Tibet) in the end-Neoproterozoic to Ordovician Indian margin of Gondwana. *Precambrian Res.* **2020**, *348*, 105865. [CrossRef]

Disclaimer/Publisher's Note: The statements, opinions and data contained in all publications are solely those of the individual author(s) and contributor(s) and not of MDPI and/or the editor(s). MDPI and/or the editor(s) disclaim responsibility for any injury to people or property resulting from any ideas, methods, instructions or products referred to in the content.